Journal of Inorganic and Organometallic Polymers and Materials (2022) 32:614–630
https://doi.org/10.1007/s10904-021-02142-7

Green Synthesis of Zinc Oxide Nanoparticles (ZnO NPs) for Effective Degradation of Dye, Polyethylene and Antibacterial Performance in Waste Water Treatment

Vinay B. Raghavendra[1] · Sushmitha Shankar[2] · M. Govindappa[3] · Arivalagan Pugazhendhi[4] · Minaxi Sharma[5] · Siddaiah Chandra Nayaka[2,6]

Received: 22 August 2021 / Accepted: 23 October 2021 / Published online: 1 December 2021

Abstract

At present, there is a vital need for river water purification by developing new approaches to eliminate bacterial biofilms, textile dyes, and Low-Density Polyethylene (LDPE) plastics that pose severe threats to human and environmental health. The current work put forward the construction of an eco-friendly green strategy to synthesize zinc oxide nanoparticles (ZnO NPs) using areca nut (*Areca catechu*) extract and their application to tackle the challenges in water purification. Prepared biogenic NPs were characterized by X-ray diffraction analysis (XRD), Fourier Transform Infra-Red (FT-IR), Energy Diffraction Spectroscopy (EDS), Scanning Electronic Microscopy (SEM), Transmission Electron Microscopy (TEM) analysis, confirmed the spherical shape in 20 nm and UV–vis spectroscopy. The characteristic absorption band exhibited at 326 nm confirmed the formation of ZnO NPs using UV–vis spectroscopy. Among all the tested bacterial pathogens, the *E. coli* at 50 µg/mL concentration showed the highest inhibition of biofilm activity, followed by the highest growth curve, cellular leakage, and potassium ion efflux. The ZnO NPs observed with photo-degradation of Rhodamine-B (Rh-B), Methylene Blue (MB), and Nigrosine dyes under sunlight irradiation at different time intervals. Finally, the photocatalytic activity of LDPE-ZnO NPs nanocomposite film showed the highest degradation under solar light irradiation were confirmed through photo-induced weight loss, SEM, FTIR, and MALDI-TOF analysis. This study demonstrates ZnO NPs exhibit efficacy against biofilm formation, degradation of photocatalytic textile dyes, and low-density LDPE film under solar light irradiation, which can be a step forward in water purification.

Keywords Areca nut · ZnO NPs · Antibacterial activity · Anti-biofilm activity · Photocatalytic activity · Low-density polyethylene

✉ Siddaiah Chandra Nayaka
moonnayak@gmail.com

Vinay B. Raghavendra
viragh79@gmail.com

Arivalagan Pugazhendhi
pugal.smile@gmail.com

[1] P.G. Department of Biotechnology, Teresian College, Siddarthanagar, Mysore 570011, India

[2] Institute of Excellence, Vijnana Bhavan, University of Mysore, Manasagangotri, Mysore 570006, India

[3] Department of Studies in Botany, Davangere University, Shivagangotri, Davanagere 577 007, Karnataka, India

[4] Innovative Green Product Synthesis and Renewable Environment Development Research Group, Faculty of Environment and Labour Safety, Ton Duc Thang University, Ho Chi Minh City, Vietnam

[5] Department of Applied Biology, University of Science and Technology, Meghalaya 793101, India

[6] Department of Studies in Biotechnology, University of Mysore, Manasagangotri, Mysore 570006, India

1 Introduction

Water is an essential compound, and its availability is necessary for human beings and other living organisms to live. On the other side, the earth's water suffers from several major environmental and bio-hazards such as pathogenic microorganisms, industrial wastes, plastics, and other toxins added into the water during rain, leading to water pollution. Among these, biofilm formation, textile or industrial dyes, and plastics are the major problems. According to the available statistics, approximately per year, 10,000 types of synthetic and hazardous dyes have been used in industries worldwide. Usage of hazardous dyes and derivatives of organic pollutants, which are extensively used in textile, paper, and leather industries, directly enter into mainstream river water which leads to severe toxic, carcinogenic and mutagenic characters [1]. Elimination of these organic pollutants from river stream has now gained attention towards researchers. Further, the dyes and organic pollutants contain a wide range of chemical structures, mainly aromatic compounds. The commonly practiced methods adopted for removal of synthetic dyes such as coagulation, flocculation, membrane separation, catalytic degradation, chemical reduction, activated charcoal adsorption, and biodegradation [2].

Another major issue found in river streams is the formation of biofilms formed by the accommodation of millions of planktonic microorganisms. Biofilm causes several infections in humans, including the eye, ear, gastrointestinal tract, lungs, urogenital, teeth, and other organs [3].

Low-density polyethylene (LDPE) is widely used to manufacture various products such as water bottles, dispensing bottles, wash bottles, plastic bags, and equipment's which are accumulating at a rate of 25 million tons per year [4]. However, disposal of million tons of non-degradable petroleum-based plastic waste was manifested into the ocean may have posed a severe threat to the marine environment. There are various kinds of nanomaterials, which carried the vast potential to treat polluted water, which is very effective due to their unique properties such as more significant surface area, ability to work at a lower concentration, etc. [5]. Metal nanoparticles are known to emerge in recent years owing to their expansion in biomedical and environmental applications. Nanosized metal nanoparticles have gained immense attention in recent years, owing to their desirable properties with diverse applications, such as catalysts, [6], sensors [7] and photoelectron devices [8]. Numerous nanosized metal nanoparticles such as Fe_3O_4, TiO_2, MgO, CuO, and ZnO have been expanded for their potential in photocatalytic water remediation and varied biological applications [9, 10].

Among various semiconductor metal NPs, Zinc oxide (ZnO) exhibits multifaceted roles with multiple applications owing to its eco-friendly nature. ZnO is known to exhibit varied effects [11, 12]. Zinc oxide nanoparticles have shown several morphological types like nanosheets, nanorods that make them excellent material for water treatment, and bactericidal agents [13]. ZnO provides a direct wide bandgap and photocatalytic activity to expel toxic chemicals from the environment [14]. ZnO nanoparticles also help in delivering antibiotics to specific sites, especially biofilm-forming pathogens [15]. They are utilized to remove toxic agents from wastewater as they exhibit a large surface area by volume ratio compared to bulk materials [16]. Green synthesis routes are eco-friendly and utilize lower toxic methods include natural resources like microorganisms, algae, plant sources, etc. Plants are known to exhibit superiority over other biological sources for the large-scale production of metal nanoparticles. Various phytoconstituents like alkaloids, terpenoids, proteins, flavonoids, and carbohydrates present in the plants could aid in the bioreduction and stabilization process in metal nanoparticles [17].

Nanoparticles produced using medicinal plants extracts are one of the simplest and easiest approaches. Ganguly et al. [18] reported the green synthesis of silver nanoparticles from *Bacopa monniera* has reduced synthetic dyes because of the high content of saponins present in Brahmi leaf.

Areca catechu L. is also known as betel nut, which belongs to the family Arecaceae. In India, it is commonly used as anthelmintic material for chewing and traditional herbal medicine to cure gastrointestinal and parasitic diseases [19]. Due to the presence of novel phytochemicals in betel nut has been reported as an anticancer, anti-depressant, analgesic, anti-oxidant, anti-inflammatory, anti-aging, and plasma cholesterol-lowering agent [20]. Therefore, there is a need to search for an eco-friendly and nanotechnological approach for anti-biofilm and photocatalytic degradation of LDPE.

The current work deals with the synthesis of zinc oxide nanoparticles using Areca nut water extract. The zinc oxide nanoparticles thus produced are characterized and evaluated for their antibiofilm formation activity and capacity of photodegradation of dyes. ZnO NPs nanoparticles were investigated for their photocatalytic degradation under solar light in the presence of air and the absence of light degradation under solar.

2 Materials and Methods

2.1 Areca Nut Boiled Extract Preparation

The fresh areca nut, were collected from *Areca catechu* plantation in Hassan district, Karnataka, India. Fresh and ripened areca nut were stored in polythene bags to the laboratory and

kept for further use. Around 20–25 areca nut were taken, and outer shells were removed with the help of a scalpel and made into small pieces. The cut material was washed with running tap water and soaked in a 500 mL Erlenmeyer flask containing 250 mL of deionized water. The mixture was heated to boil for around 30 min and then cooled at room temperature. Finally, it was filtered using Whatman number-1 filter paper. The resultant filtrate was stored at 4 ℃ for future studies [21].

2.2 Synthesis of ZnO NPs

80 mL areca nut extract was added into a 250 mL conical flask containing 1 mM zinc nitrate {Zn $(NO_3)_2 \cdot 6H_2O$} (Sigma-Aldrich, India) aqueous solution (20 mL). The reaction mixture was kept in a magnetic stirrer for one h maintaining an even stirring. Centrifugation of the reaction mixture was carried out at 12,000 rpm for 10 min for room temperature, and later calcination was carried at 400 ℃ for 120 min. Finally, a yellow solid product was collected and rinsed with distilled water. The synthesized ZnO NPs dried and separated from the colloidal solution were maintained in air-tight containers and used further [22].

2.3 Characterization of Biosynthesized ZnO NPs

The Characterization of ZnO NPs for their optical properties based on UV-spectra measured at a wavelength of 300–500 nm. The purity and crystal nature of ZnO NPs was analysed on an XRD operating at 30 kV, and 40 mA was used to check the quality and crystalline nature of ZnO NPs. FTIR analysis of ZnO NPs was performed to determine the functional groups responsible for bioreduction and stabilization of nanoparticles at a resolution of 4 cm − 1. DLS elemental compositions of the photosynthesized ZnO NPs were performed using Energy Dispersive X-ray diffraction (EDAX). SEM (JSM-5600LV, JEOL) was used to know elemental analysis as described previously [23].

2.4 Antibacterial Activity of Synthesized ZnO NPs

The antibacterial effect of biogenic ZnO NPs was carried out using the disc diffusion method against bacterial pathogens *Pseudomonas aeruginosa*, *Staphylococcus aureus, Escherichia coli,* and *Bacillus subtilis,* at bacterial cultures concentrations of 1.5×10^8 CFU/mL. Fresh bacterial overnight culture of each strain was uniformly swabbed on nutrient agar plates, and 6 mm wells were bored onto the individual Petri plate. One well was loaded with 25 µL of ZnO NPs solution, streptomycin solution was loaded as standard, and distilled water was used as control. Plates were incubated for 24 h at 37 ℃, and all assays were conducted in triplicates, and the zone of inhibition formed around each well was measured [24].

2.5 Effect of ZnO NPs on Biofilms Formation, Growth Curve, Cellular Leakage, and Potassium Ion Efflux of *B. subtilis* and *E. coli*

In brief, antibiofilm activity was carried out using 12 well plates, where 1 mL of bacterial suspension (1 X 10^5 CFU/mL) with different concentrations of (10, 25 and 50 µg/mL) was incubated at 37 ℃ for 24 h. After the incubation period, bacterial suspension was removed, and 0.1% w/v crystal violet (HiMedia, LLC) was added and incubated for 30 min followed by removal of excess of crystal violet stain in stained cells by washing 2–3 times with distilled water followed by incubation with 30% v/v acetic acid for 15 min. Later cells retained crystal violet was examined by the extent of inhibition of biofilm formation of ZnO NPs. Finally, the absorbance was measured at 590 nm using a microtiter plate reader (Bio-Rad) [25].

The *B. subtilis* and *E. coli* were cultured in Luria–Bertani (LB) (HiMedia, LLC) broth to an optical density at 600 nm of 0.3 OD. The different concentrations (10, 25, and 50 µg/mL) of ZnO NPs were prepared and added to 96 well plates and incubated at 35 ± 2 °C for 24 h. Culture without ZnO NPs was used as control. Further, bacterial cell growth was analysed by reading the OD at 600 nm at 30 min time intervals using a microplate reader. Experiments were carried out in triplicates for all the samples. The different concentrations (10, 25, and 50 µg/mL) of ZnO NPs on two bacterial species (*B. subtilis* and *E. coli*) were studied by measuring cellular material after incubation as described accordingly [26]. The log phase of two bacterial cultures was inoculated into 0.1% sterile peptone water added with different concentrations (10, 25, and 50 µg/mL) of ZnO NPs separately and without sample was considered as control. All the samples were incubated at 35 ± 2 °C for 0, 30, 60, 120,150, 180, 210 and 240 min. The optical density was measured at 260 nm in triplicates [27].

B. subtilis and *E. coli* have grown on LB broth were incubated at 37 °C. The culture was diluted to maintain its turbidity to 0.5 McFarland Standards (5×10^5 CFU/mL). Varying concentrations (10, 25, and 50 µg/mL) of ZnO NPs were tried on biofilms production of both the bacteria as described earlier [27]. The different concentrations (10, 25, and 50 µg/mL) of ZnO NPs were studied on membrane damage of bacterial cells by measuring the potassium efflux [28]. Triplicates were maintained, and all the experiments were conducted thrice.

2.6 Photocatalytic Degradation of Textile Dyes

Photocatalytic activity of ZnO NPs (100 µg) was evaluated for the degradation of Rhodamine-B (Sigma-Aldrich) (10 µM), Methylene Blue (Sigma-Aldrich) (10 µM), and Nigrosine (Sigma-Aldrich) (10 µM) under direct sunlight [29]. The reactions were analysed using UV–Vis spectroscopy. The reaction mixture was filtered, and maximum absorbance obtained (λmax = 660 nm, 543 nm, and 570 nm) at varied time span were noted.

2.7 Photocatalytic Degradation of Low Density Polyethylene (LDPE) Films using ZnO NPs

2.7.1 Preparation of ZnO Nanocomposite Films

ZnO nanocomposite film samples were prepared accordingly [30]. Prepare the stock mixture of the polymer by dissolving 0.5 g of Polyethylene- low density (Sigma-Aldrich) (particle size 1000 micron) in 50 mL of cyclohexane anhydrous 99% (Sigma-Aldrich) maintained at 70 °C under vigorous mixing for 60 min. Later, ZnO NPs were evenly mixed in the above 50 mL solution to give 500 µL (wt %) ZnO NPs regarding the overall mass of LDPE. Later spread this on a glass slide (7 cm × 2 cm) followed by drying for 20 min at 70 °C and 48 h at room temperature to acquire a thin LDPE- ZnO NPs.

2.7.2 Photocatalytic Performance Test

The photocatalytic degradation of LDPE exposed to solar irradiation under ambient conditions was performed using ZnO NPs. Later, LDPE alone and LDPE treated with ZnO NPs film sample of dimension 2 cm × 4 cm were taken and kept in a Petri plate were exposed to solar irradiation under ambient conditions to probe the photocatalytic activity on every sunny day for a period of 300 h. The degradation efficiency of the ZnO NPs was calculated using the following Eq. (1).

$$Degradation\,\% = \frac{WL_s - WL_d \times 100}{WL_s} \quad (1)$$

where, WL_s is the weight loss of solar irradiated nanocomposite in the presence of solar light and WL_d is the weight loss of in the absence of solar light irradiation (dark) after exposure period of 300 h according to Olajire et al. [31].

2.8 In situ Biodegradation Assay

Taking the lead from the enhanced biodegradation part. The LDPE film was treated with ZnO NPs under in vitro conditions, and the biodegradation was tested under natural conditions. Topsoil was obtained by digging a barren land, and LDPE (solar), LDPE-ZnO NPs (solar), LDPE (dark), and LDPE-ZnO NPs (dark) nanocomposite films of dimensions (2 cm × 4 cm) were subjected to sterilization with 70% ethanol for 10 min. These were kept below the soil's surface in the vertical position at a depth of 1 inch and the same distance apart [32]. Proper moisture and aeration conditions were maintained regularly for two weeks at intervals. Uninoculated soil with LDPE film coupons was taken as the negative control. Recovery of degradation and analysis of LDPE film samples from the soil was carried at intervals of 1, 2, and 3 months according to Gupta et al. [33].

2.9 Tensile Strength Testing

Tensile testing was conducted to determine the strength of LDPE films. The tensile strength measurements were tested using Universal testing machine. LDPE films with 30 mm length and 10 mm width were cut into pieces and run into a speed of 1 mm/min for measuring tensile strength calculated for its elongation using following formula

$$\text{Tensile strength} = \frac{\text{Load at break}}{\text{Original width} \times \text{Original thickness}} \quad (2)$$

Percent elongation is measured by using following equation:

$$\%\ \text{Elongation} = \frac{\text{Elongation at rupture } \times 100}{\text{Initial gage lenght}} \quad (3)$$

Surface sterilized samples were further analysed for FT-IR, and SEM, as described earlier [34]. The pure LDPE samples and LDPE-ZnO NPs nanocomposite samples were characterized for their weight loss, FT-IR, SEM, and Mass Spectrometry analysis. The molecular weight of bioreagents was analysed using Kompact (SEQ) KRATOS analytical time of flight mass spectrometry and MALDI (Matrix Assisted Laser Desorption/Ionisation) technique [34].

3 Results and Discussion

3.1 Synthesis and Characterization of ZnO NPs

ZnO NPs exhibit unique optoelectronic properties, due to which they have gained innumerable attention nowadays. The preliminary sign of nanoparticles synthesis is its visual change in the color of the solution formed. The presence of $\{Zn\ (NO_3)_2{\cdot}6H_2O\}$ and the aqueous extract's physicochemical differences can be determined by a change in the color of the solution. Thus, the color change from dark

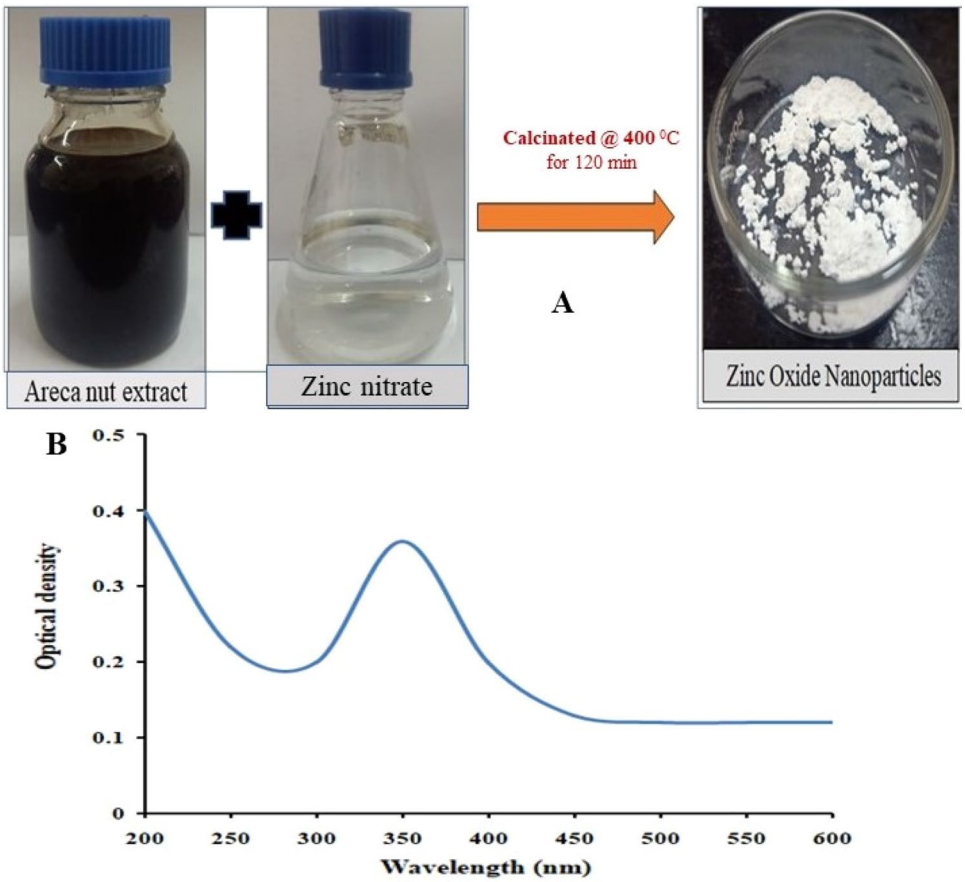

Fig. 1 **A** Areca nut water extract with zinc nitrate, thus, forming the colour change from dark wine color to white precipitate **B** UV–visible spectra obtained for biosynthesized ZnO NPs were observed at 346 nm

wine to white precipitate followed by calcination at 400 °C for 120 min represents the synthesis of ZnO NPs (Fig. 1A). After calcining at 400 °C, the areca nut extract consists of bioactive molecules, which help in the nucleation process known to play a role in reducing Zn ions into ZnO NPs [35]. The synthesis was further confirmed with the aid of UV–Vis spectros copy analysis. The characteristic absorption band that appeared at 346 nm confirmed the synthesis of ZnO NPs as shown in (Fig. 1B). The present findings are in the same trend was observed with previous reports of ZnO NPs synthesized from plants [35].

3.2 Characterization of ZnO NPs

FTIR analysis of synthesized ZnO NPs spectrum showed vibration peaks at 1739.98, 1503.22, 1380.65, 831.29, 707.46, 583.55, and 405.18 cm^{-1} as shown in (Fig. 2A). This exemplifies the Alkynes HC-H, stretch C-H (medium)-Alkanes CH_2, C = C (medium to weak)-Alkynes C = C Stretch, C = N (medium)-Amides-NH, C-H-Alkynes- C-H bond, C-H-Alkyl halides-C–Br stretch, C-H-Alkynes –C-H bend, C-H- Alkynes –C-H bend, C = C- Alkynes –C-H bend, C = C- Alkynes –C-H bend respectively. The results of FTIR spectra reveal the presence of alkyl halides, amine, alkynes, and alcohols. Here the presence of protein molecules in the areca nut extract may be responsible for the possible reduction of metal ions. A similar banding pattern was also reported by Natarajan et al. [36]. Overall, results suggest that the flavonoids, the protein molecules, and their functional groups play a vital role in the bioreduction of zinc salts and the capping of ZnO NPs [37]. The zeta potential of the ZnO NPs was found to be 7.1 mV and polarity was found to be positive, and surface charged nanoparticles and physical properties were analyzed based on zeta potential. The elemental composition of the ZnO NPs using EDX showed peaks which were situated between 1.2 and 8.8 keV with the presence of elements like C, O, Al and Zn, in the ZnO nanostructures were found to be 54.1, 32.3, 0.7, and 12.9% by atomic mass, respectively as shown in (Fig. 2B). Furthermore, one additional peak of Al was also found. The presence of C indicates the biomolecules presence in extracts as capping agents during the formation of the ZnO NPs. The surface morphology and crystalline nature of the ZnO NPs were investigated through X-ray diffraction studies [38]. The XRD patterns of the ZnO NPs exhibited

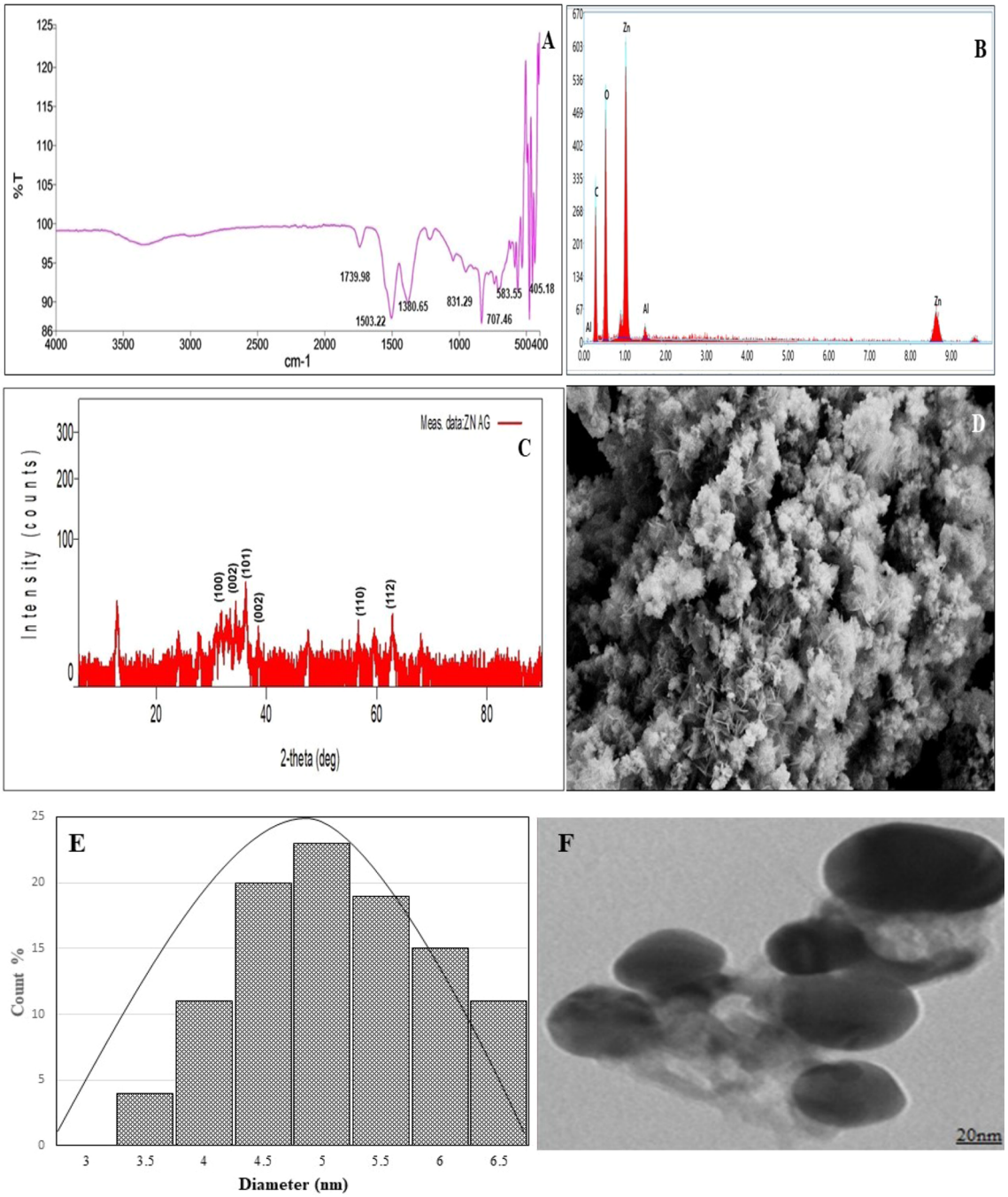

Fig. 2 Characterization of ZnO NPs. **A** FTIR spectrum of ZnO NPs **B** EDAX spectra of ZnO NPs, **C** XRD pattern of the synthesized ZnO NPs **D** SEM images showing shape and distribution of ZnO NPs (**E**) Histogram of size of the ZnO NPs showing 5 nm (**F**). TEM images showing the spherical shape of ZnO NPs at 20 nm

2θ values at 31.84°, 34.52°, 36.33°, 47.63°, 56.64°, 62.91°, 66.54°, and 69.12°, corresponding to (100), (002), (101), (102), (110), (103), (200), (112) and (201) planes of hexagonal as shown in (Fig. 2C). This also matched well with wurtzite structure (JCPDS card no.: 36–1451) compared to previously synthesized ZnO NPs [39]. The nanostructure of synthesized ZnO NPs was seen in SEM were of almost similar sizes as shown in (Fig. 2D). SEM images revealed the size of ZnO NPs as nm. Our results indicate spherical and hexagonal structures of an average size of 5 nm in size. Size of the nanoparticles were presented through histogram as shown in (Fig. 2E). From TEM analysis, the size and morphology were evaluated and demonstrated the spherical shape images are represented in 20 nm as shown

Table 1 Antibacterial activity of ZnO NPs on different bacterial cultures

Bacteria	Areca nut extract	Control (DW)	Antibiotic	ZnO NPs (in cm)
Staphylococcus aureus	0.8 ± 0.70	0	1.3 ± 0.45	0.5 ± 0.70
Pseudomonas aeruginosa	0.5 ± 0.45	0	1.5 ± 0.25	0.4 ± 0.45
Bacillus subtilis	2.0 ± 0.25	0	3.5 ± 0.25	2.5 ± 0.25
Escherichia coli	2.3 ± 0.75	0	3.2 ± 0.25	2.4 ± 0.75

Repeated each experiment thrice by maintaining three replicates

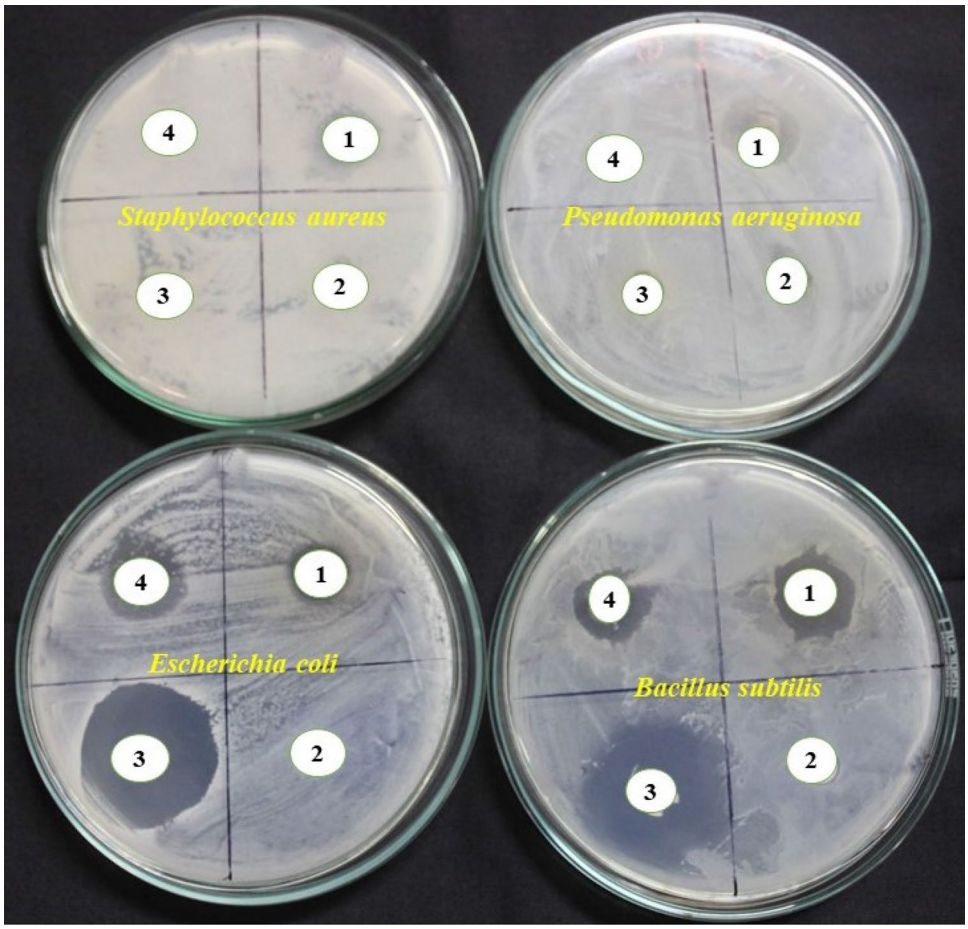

Fig. 3 Antibacterial activity of ZnO NPs against various clinically important bacterial species. *S. aureus*, *Pseudomonas aeruginosa, B. subtilis* and *E. coli*, representing (1) Areca nut extract (2) Control (3) Antibiotic (4) ZnO NPs

in (Fig. 2F). The results demonstrated the formation of smaller sized ultrafine ZnO nanoparticles. Usually, green synthesized ZnO NPs containing phytoconstituents and products contain spherical, triangular, cubic, or hexagonal sizes ranging between 5–30 nm [40].

3.3 Anti-Bacterial Activity of ZnO NPs

The ZnO NPs have shown significant antibacterial activity, with maximum growth inhibition activity was found *in E. coli* (2.4 cm) and *B. subtilis* (2.5 cm) followed by *S. aureus* (0.50 cm) and *P. aeruginosa* (0.4 cm) were compared with the standard antibiotic, areca nut water extract alone and control as shown in Table 1 and (Fig. 3). The zone of inhibition of different bacterial pathogens against the biosynthesized ZnO NPs is represented as the mean values of triplicates. ZnO NPs inhibited maximum growth in *B. subtilis* and *E. coli*. Studies have shown that ZnO NPs inhibit the growth of microbes by permeation through the cell membrane [41]. Rao et al. [42] reported the Antibacterial activity from silver nanoparticles (Ag-NPs) in polyelectrolyte hydrogels reveals the highest inhibition towards gram-positive *S. aureus* and gram-negative *E. coli*. The AgNPs coated with chitosan layer of the composite scaffold were evaluated for the efficacy against gram positive and gram negative bacterial strains [43]. Metallic nanoparticles reveal promising approach for the controlling microbial

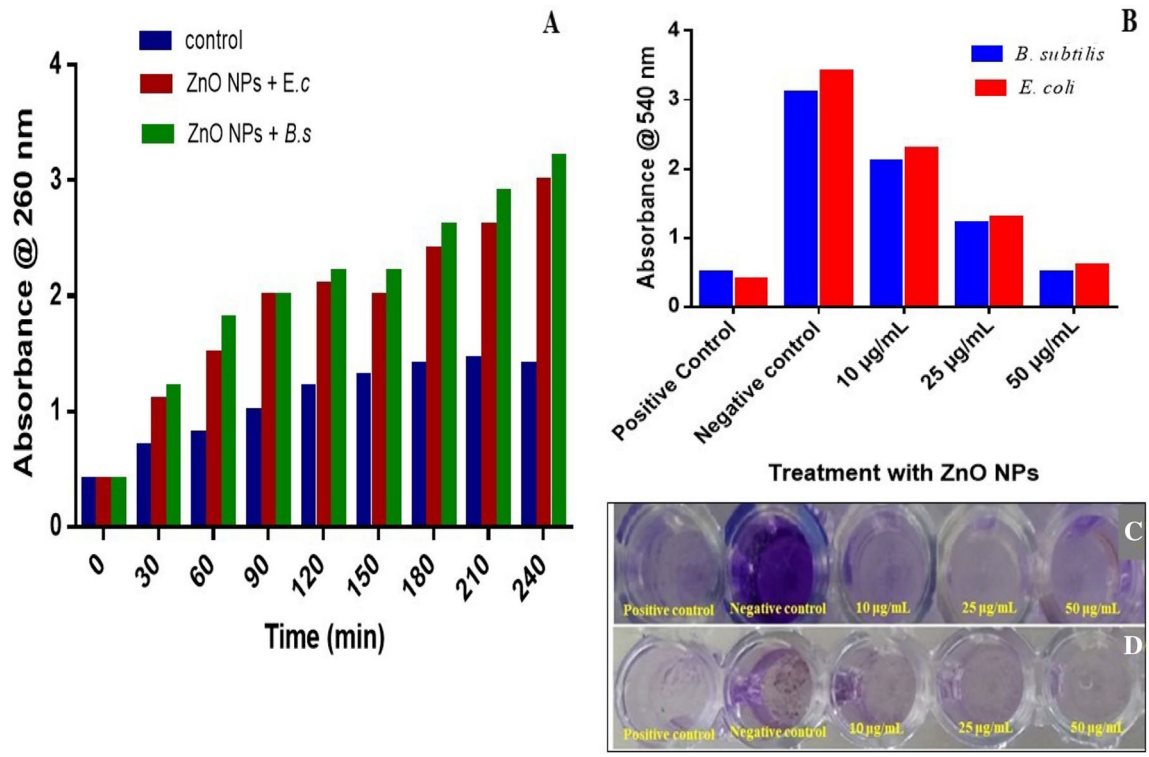

Fig. 4 The ZnO NPs showed significant anti-biofilm assay. (**A**) Represents the Anti-biofilm assay and showed highest biofilm activity at 240 min by *E. coli*. (**B**) Anti-biofilm activity showing least activity at 50 µg/mL concentration of *E. coli*. (**C**) Showing highest thickening of *B. subtilis* observed at different concentrations. (**D**) *E. coli* showing less thinning of bacterial formation at different concentrations

pollution in drinking water, therefore biosynthesis of metal nanoparticles is of considerable interest in the treatment of waste water [44, 45].

3.4 Effect of ZnO NPs on Biofilm Formation Against *B. subtilis* and *E. coli*

ZnO NPs were evaluated for the formation of biofilm against *B. subtilis* and *E. coli* at different time intervals. Among them, ZnO NPs treated with *E. coli* revealed very prominent eradication of formation of biofilm activity at 240 min, whereas *B. subtilis* showed significantly less eradication of formation of biofilm at 240 min when compared with *E. coli* as shown in (Fig. 4A). The microbial biofilm inhibition potential of ZnO NPs at different concentrations (10, 25, and 50 µg/mL) on *B. subtilis* and *E. coli*. Among the, *E. coli* at 50 µg/mL concentration showed the highest inhibition of biofilm activity when compared with *B. subtilis* at 50 µg/mL as shown in (Fig. 4B). Anti-biofilm assay was studied using crystal violet staining technique against biofilm-forming bacteria *E. coli* and *B. subtilis*. *B. subtilis* showed thick films of bacterial cells at 50 µg/mL as shown in (Fig. 4C). Furthermore, *E. coli* at 50 µg/mL showed a thin biofilm of bacterial cells, which was carried out at 12 well plates. Moreover, biofilms are the thick film of bacterial cells formed over living surfaces due to cell colonization, causing significant environmental and health issues. Biofilms are microorganisms associated with extracellular polymer substance which contains polysaccharides, extracellular DNA, proteins, and water [46]. The ZnO NPs significantly inhibited the biofilm formation of *B. subtilis* and *E. coli* in a dose-dependent manner. Hsueh et al. [47], reported that surface structures of *B. subtilis* biofilm became smooth under lower concentrations of ZnO NPs, significantly reduced biofilm formation activity. A similar observation was reported showed antibiofilm activity against *Aeromonas hydrophila* showed the highest inhibition activity from laminarin formulated gold nanoparticles at 100 µg/mL. The efficacy of silver nanoparticles against *P. aeruginosa* with the highest reduction rate in biofilm production might be because of the extracellular matrix of polymeric substance [48–50]. AgNPs played the key role in catalytic reduction and bactericidal activity. Moreover, the prepared hydrogel has enough robust to withstand cyclic stress, uniaxial stress and oscillatory stress which have been extensively justified by the physico-mechanical characterizations [51].

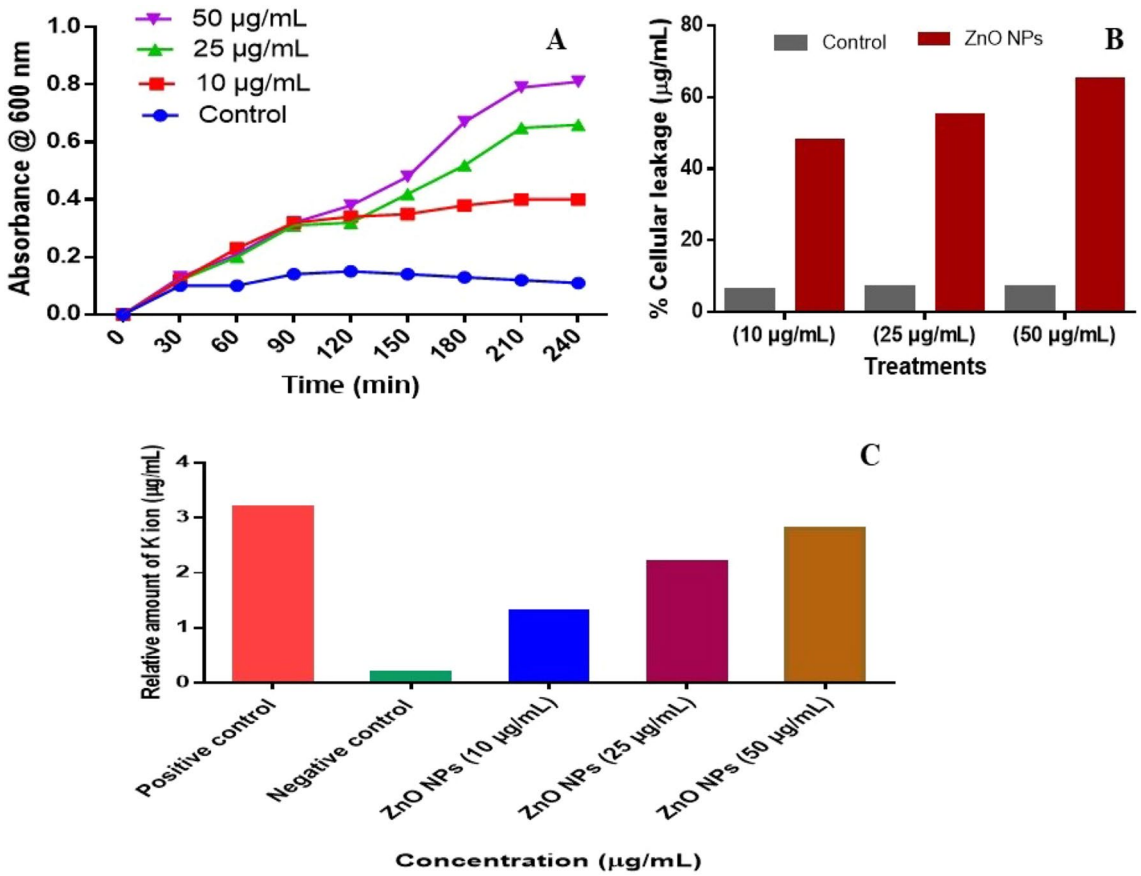

Fig. 5 Effect of ZnO NPs on growth curve, cellular leakage and potassium ion efflux of *E. coli*. (**A**) Growth curve showing *E. coli* at different time intervals. (**B**) The effect of ZnO NPs treatment against *E. coli* and showed highest cellular leakage at 50 µg/mL. (**C**) The effect of ZnO NPs against *E. coli* and showed highest potassium efflux at 50 µg/mL

3.5 Effect of ZnO NPs on Growth Curve, Cellular Leakage, and Potassium Ion Efflux of *E. coli*

Based on the results obtained on the anti-biofilm formation growth curve, cellular leakage and potassium ion efflux were carried out on *E. coli*. A gradual decrease in the growth curve of *E. coli* at 240 min time treated with varying concentrations (10, 25, and 50 µg/mL) of ZnO NPs is as shown in (Fig. 5A). Studies by Fattah et al. [52] have reported various concentrations (50–150 g/mL) of silver nitrates showing strong inhibitions of *Klebsiella granulomatis*, *Pseudomonas aeruginosa*, and *Escherichia coli* in a paint-AgNP admixture. Based on concentration-dependent, the ZnO NPs showed more release of cellular leakage when treated with higher concentration (50 µg/mL) of ZnO NPs as shown in (Fig. 5B). The elevated use of cellular material mainly depended on the incubation period and dose, which may be in turn because of the effect of ZnO NPs [53]. The efflux of potassium ions of *E. coli* was increased due to the toxicity of ZnO NPs at higher concentrations (50 µg/mL), as shown in (Fig. 5C). The schematic diagram (Fig. 6) explains the overall antibacterial mechanism of was as described by Govindappa et al. [49]. In nature, the bacterial cells are very active in metabolically and cytoplasmic membranes. The ZnO NPs may damage the bacterial cells anatomically, cytoplasmic membrane, DNA, and cellular materials by releasing potassium ions. The ZnO NPs significantly cause an effect on the release of cellular materials and the cytoplasmic membrane of *B. subtilis* [54].

3.6 Photodegradation Studie

The catalytic effect of green ZnO NPs was analysed by the degradation index of Rh-B, MB, and Nigrosin dyes under sunlight irradiation. The degradation of the dyes was observed by the change in color on the addition of the ZnO NPs. The solution of Rh-B showed 95% degradation changes from dark pink to pale pink and later turned colorless after 120 min, as shown in (Fig. 7A). Overall degradation of Rh-B

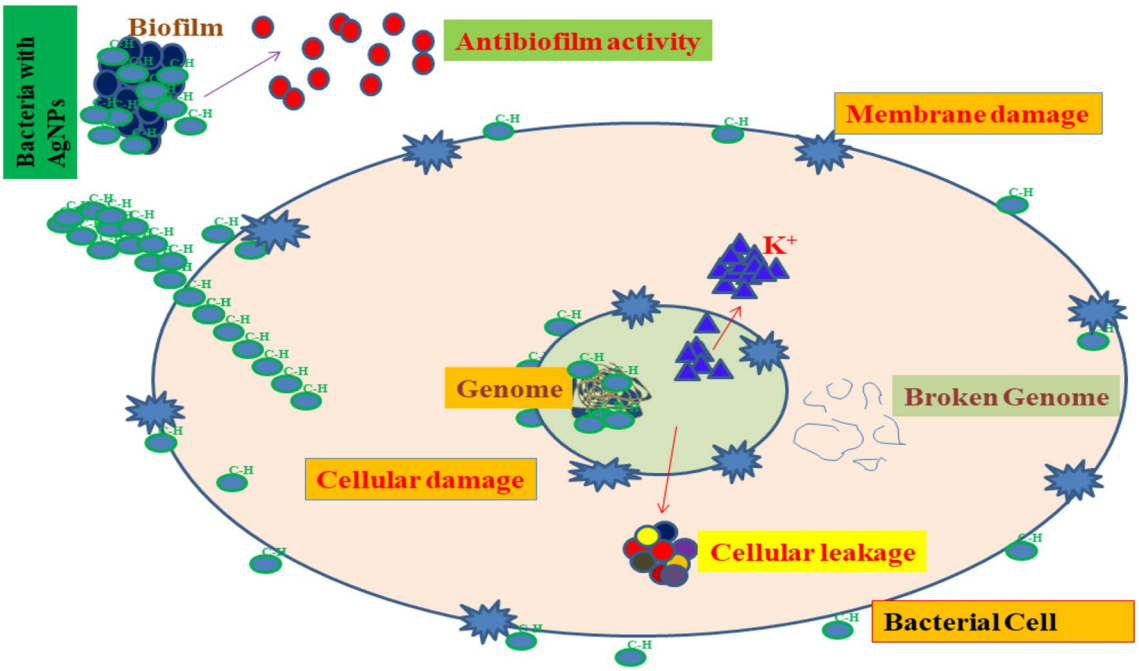

Fig. 6 Overall antibacterial mechanism of ZnO NPs based on the results obtained (Govindappa et al. 2021)

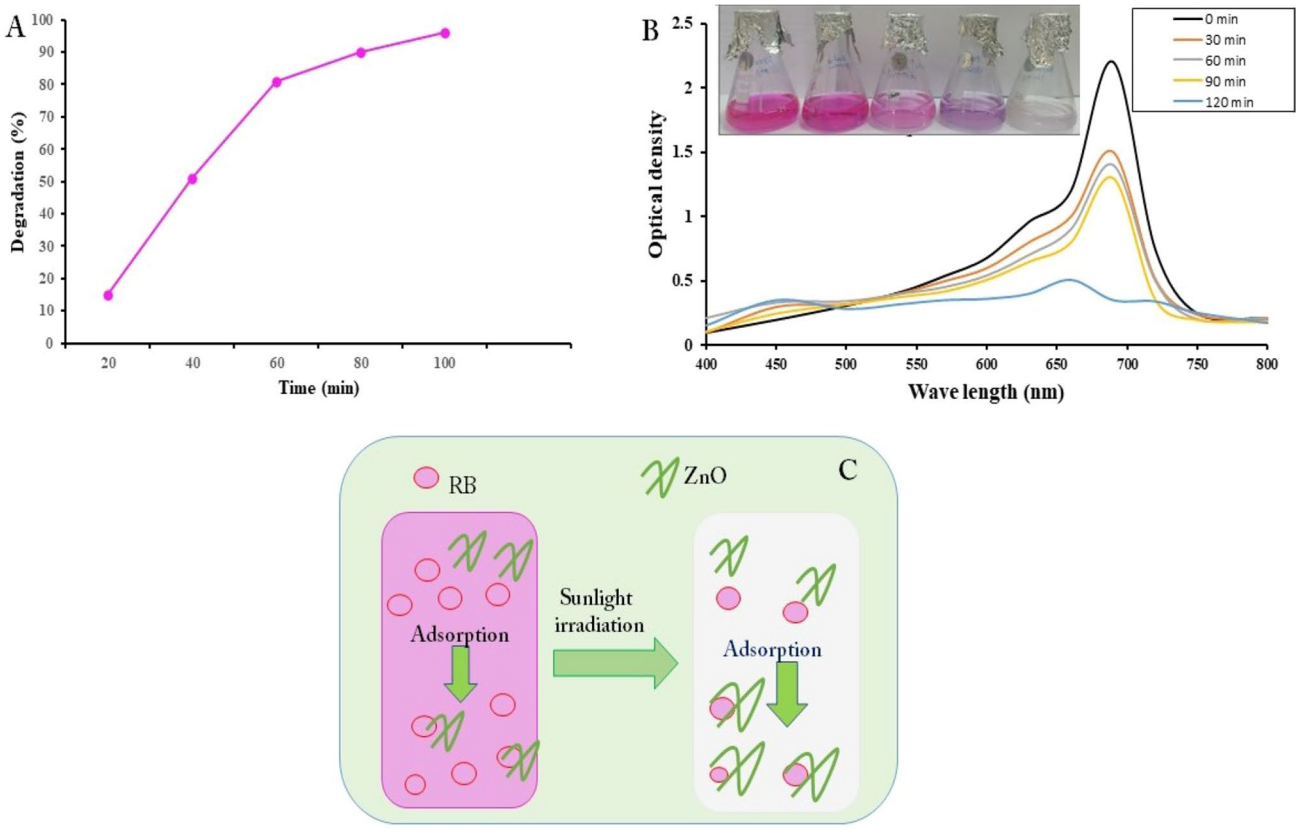

Fig. 7 Photocatalytic studies of ZnO NPs on the degradation of (**A**) Rhodamine-B dye showing 97% degradation. (**B**) Highest degradation at 120 min. (**C**) Schematic diagram showing the mechanism of degradation

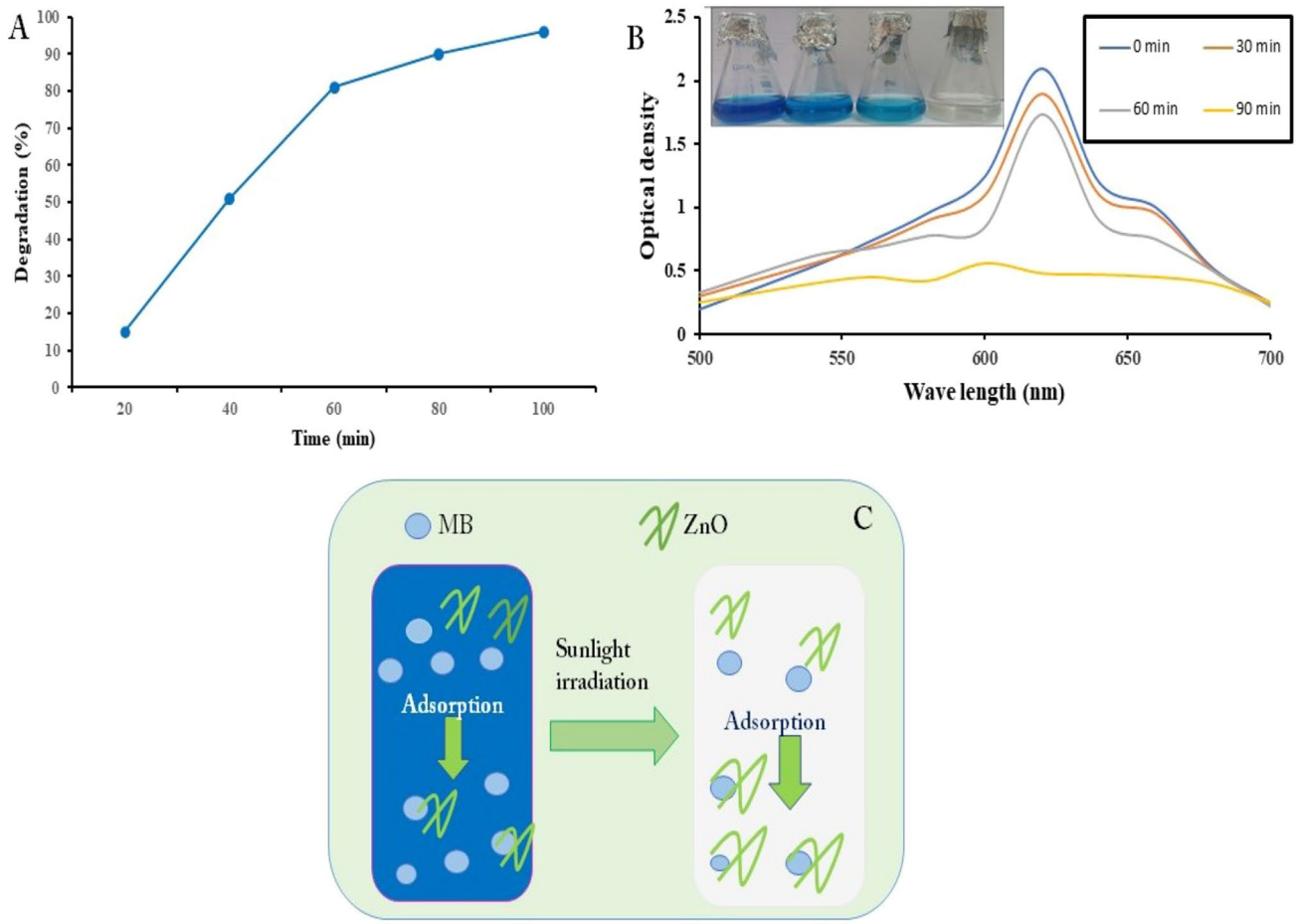

Fig. 8 Photocatalytic studies of ZnO NPs on the degradation of (**A**) Methylene blue dye showing 95% degradation (**B**) Highest degradation at 90 min (**C**) Schematic diagram showing the mechanism of degradation

changes to colorless at 120 min as shown in (Fig. 7B) and schematic diagram showed the mechanism of degradation of dye as shown in (Fig. 7C). The solution of MB dye changed from light blue to colorless after 90 min of incubation and showed 95% degradation as shown in (Fig. 8A and B). The schematic diagram showed the mechanism of degradation of dye as shown in (Fig. 8C).

In contrast, the acid black color of nigrosin showed 96% degradation and turned colorless within 90 min in the presence of ZnO NPs, as shown in (Fig. 9A and B). The schematic diagram showed the mechanism of degradation of dye as shown in (Fig. 9C). There was a gradual decrease in the peak intensities with respect to the duration of sunlight exposure for the dyes at different time intervals, respectively (Fig. 10A). Absorption peak centered at 660, 543 and 570 nm for all Rh-B, MB, and nigrosin dye in the visible region was diminished and eventually disappeared with the increasing reaction time. ZnO NPs promote the adsorption process when nanoparticles attach to the dye slowly degrade the structure of the dye [55]. Synthesized polydopamine coated silver nanoparticles dispersed into hydrated silica released catalyst against 4-nitophenol reduced congo red degradation and potassium hexacyanoferrate (III) [56].

AgNPs coated CeO_2 nanotubes supports catalyst to mitigate toxic water pollutants in minimum time interval. Furthermore, nanocatalyst degraded 4-nitrophenol and methylene blue was measured to be $8.75\times10^{-3}s^{-1}$ and $5.88 \times 10^{-3}s^{-1}$ respectively [57]

The degradation maybe because of the large surface area and mesoscopic ability exhibited by ZnO NPs. Thus, they may utilize in developing photocatalysts for wastewater pollutants removal. ZnO NPs have also been proved to degrade several dyes present in wastewater effectively [58]. The effect of the degradation process of dyes was illustrated in the schematic diagram as shown in (Fig. 10B). First, the dye will be adsorbed on the surface of nanoparticles, and then it is exposed to sunlight irradiation to excite electrons. Reduction and oxidation occur during the reaction, and electrons

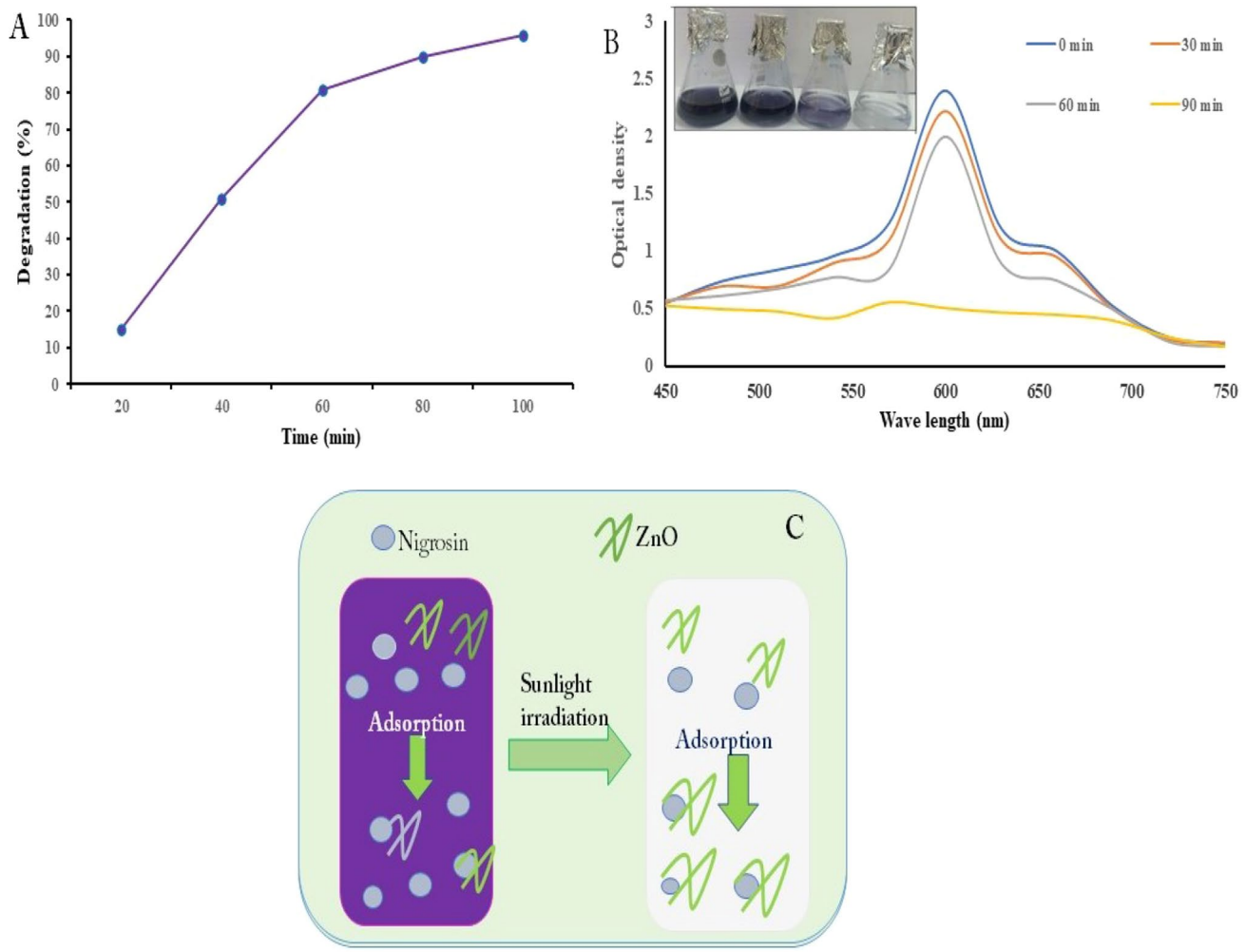

Fig. 9 Photocatalytic studies of ZnO NPs on the degradation of (**A**) Nigrosin dye showing 96% degradation (**B**) Highest degradation at 90 min (**C**) Schematic diagram showing the mechanism of degradation

may transfer from one site to another. As a result, OH- radicals and the free radicals reduce O_2 to superoxide anion O_2^- radicals and converts these degraded dye molecules into simple molecules [59]

3.7 Photocatalytic Activity of LDPE

The photocatalytic activity was carried out for LDPE and LDPE-ZnO NPs in the presence of solar light irradiation for its photoinduced weight loss, SEM, FTIR, and MALDI-TOF analysis. The weight loss of LDPE-ZnO NPs nanocomposite film steadily expanded with rising solar irradiation time to reduce a total 67% weight loss after irradiation time from 0 to 300 h. Moreover, photoinduced LDPE film under solar irradiation exhibited only 12% of weight loss at 300 h irradiation time, but LDPE and LDPE-ZnO NPs under dark condition showed only 1 and 2% of weight loss was obtained at 300 h of incubation as shown in (Fig. 11A) confirming their ability in photocatalytic degradation. LDPE films treated with ZnO NPs with solar irradiation showed maximum elongation loss and tensile strength decline after 45 days. LDPE treated with Zno NPs under dark conditions was fragile and tensile testing could not be performed on these films. Pure LDPE with solar and dark conditions did not show much elongation (Table 2). The percentage of nanoparticles that causes agglomeration in polyethylene and may cause loss of tensile strength and also alters the structure morphologically [60]. Similar results were also proved that ZnO NPs induce the degradation of LDPE film in solar light irradiation [61]. The photoinduced degradation of LDPE nanocomposite film from gold nanoparticles has been reported, which steadily increased the weight loss of 51% in 240 h under solar light irradiation in comparison with the photoinduced LDPE showing weight loss of 8.6%. Moreover, LDPE film with AuNPs gave a weight loss of only 4% under dark conditions [32]. Gupta et al. [33] reported

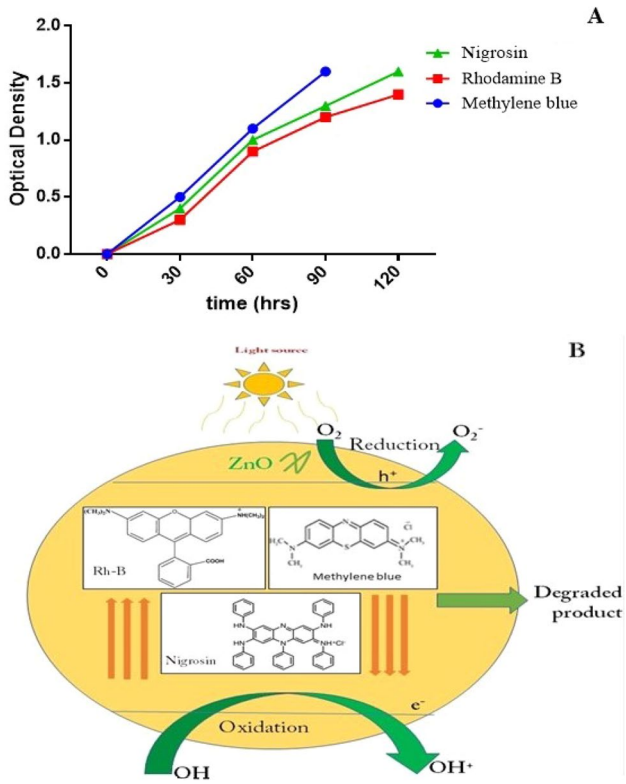

Fig. 10 (**A**) Degradation of all the three Rhodamine-B, Methylene blue and Nigrosin dye at different time intervals. (**B**) Schematic diagram showing degradation mechanism of ZnO-AgNPs based on the results obtained of all the three dyes

the degradation of polyethylene (PE) and polyvinyl chloride (PVC) showed 85% and 62% weight loss after 312 h.

3.8 Scanning Elecetron Microscopy Analysis

The surface structure of radiation-exposed polymer samples was analysed using scanning electron microscopy (SEM).

Table 2 Tensile strength and elongation values for pure LDPE and LDPE-ZnONPs films before and after visible irradiation

Sample composition	Tensile strength		Break elongation (%)	
	Before	After	Before	After
Pure LDPE (solar)	9.5	9.1	3.12	3.06
LDPE-ZnO NPs (Solar)	9.2	5.57	8.12	3.25
Pure LDPE (dark)	9.6	9.3	7.27	7.12
LDPE-ZnO NPs (Dark)	9.5	7.6	7.52	5.38

Repeated each experiment thrice by maintaining three replicates

SEM images revealed that the LDPE-ZnO NPs particles showed small cavities with 2–3 mm in size were observed in the nanocomposite film as shown in (Fig. 11B). SEM images revealed the degradation of LDPE nanocomposite film initiated through the ZnO NPs interface and led to the evolution of cavities around LDPE-ZnO NPs aggregates. The degradation of PE matrix from ZnO nanocomposites observed the formation of cavities in SEM images around polyethylene matrix [62].

3.9 FT-IR Analysis

The functional groups in LDPE and LDPE-ZnO NPs under solar light irradiation and dark condition were analysed by characteristic FTIR peaks. Figure 12 reveals FT-IR spectra of LDPE showing peaks at 3425, 2936, 1633, 1401, and 1064 cm-1. LDPE-ZnO NPs (500µL) samples after solar light irradiated for 300 h with the original samples exhibited peaks at 3544, 3558, 1216, and 816 cm − 1 corresponding to the hydroxyl group long alkyl chain. The solar irradiated LDPE-ZnO NPs samples showed lower characteristic alkyl peaks than the original LDPE sample with solar light irradiation (light). In contrast, the pure LDPE samples (dark) exhibited considerable differences. These results suggest that

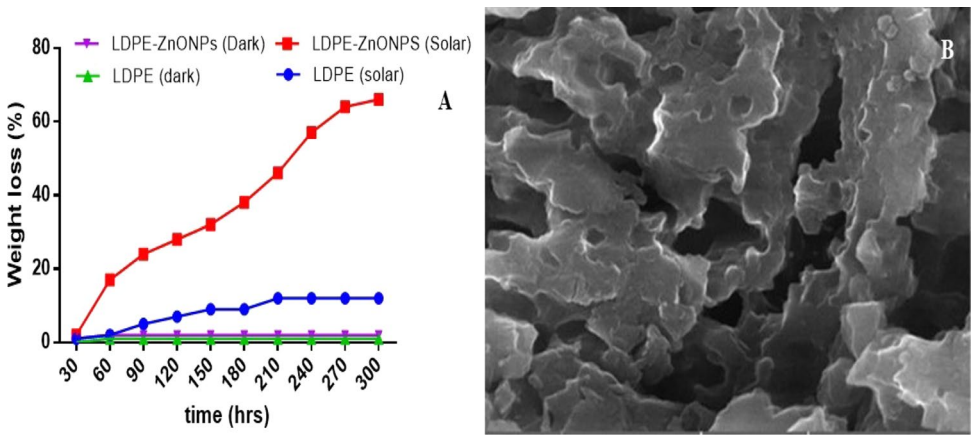

Fig. 11 (**A**) Weight loss of LDPE-ZnONPs nanocomposite film of total highest weight loss after irradiation time from 0 to 300 h (**B**) LDPE-ZnONPs particles showed small cavities with 2–3 mm in size were observed in the nanocomposite film

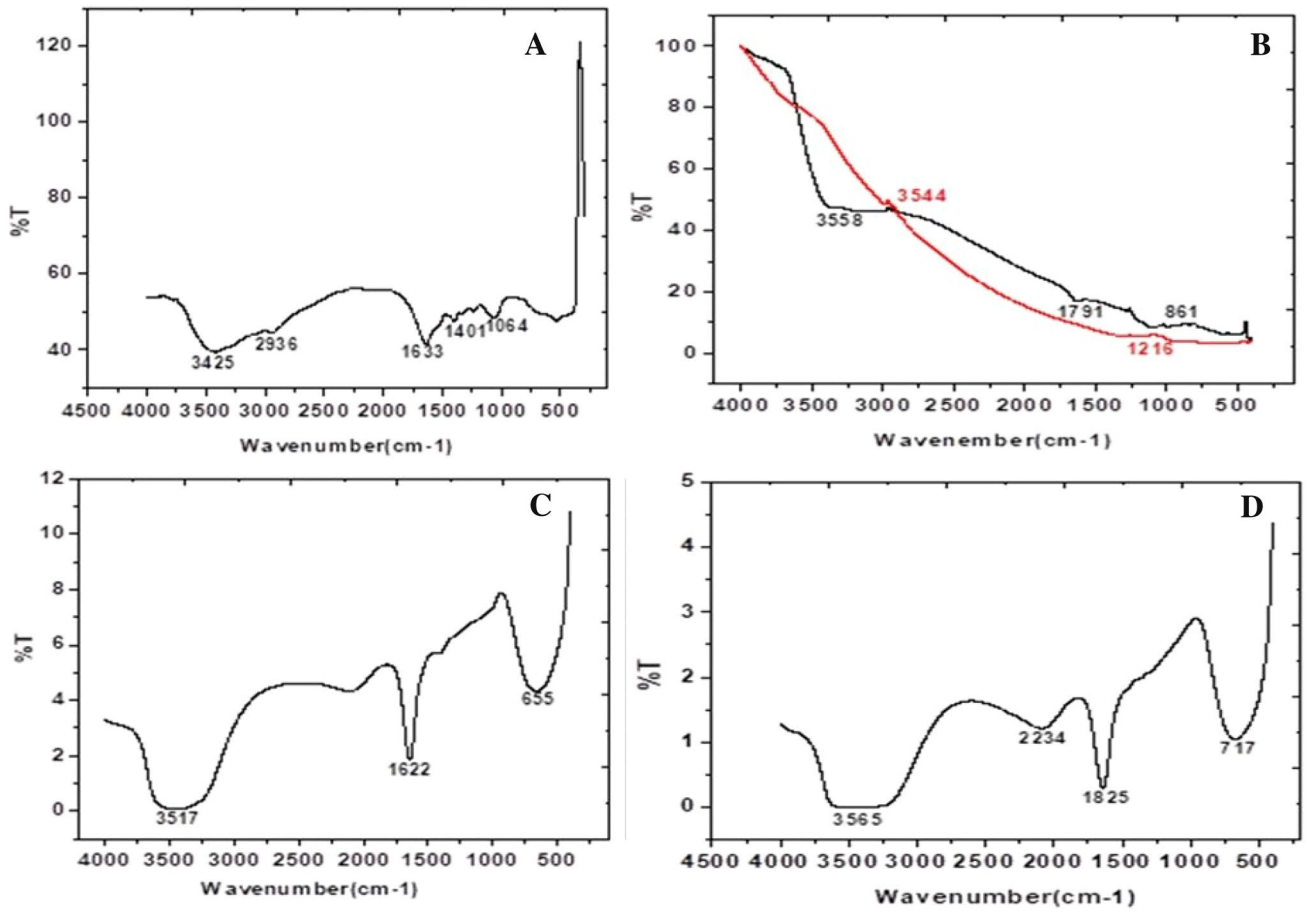

Fig. 12 (**A**) The solar irradiated LDPE-ZnONPs samples exhibited higher intensity of characteristic alkyl peaks in comparison to the original LDPE sample. (**B**) LDPE-ZnONPs at dark light exhibited lower intensity of alkyl peaks. (**C**) The degradation of LDPE-ZnONPs samples showed highest intensity in the pure LDPE samples. (**D**) The degradation of LDPE-ZnONPs showing COO or CO group, indicates the presence of carboxylic acids, carboxylates, ketones and aldehydes

the degradation of LDPE-ZnO NPs samples is almost complete and fast compared to the pure LDPE samples. Reports suggest that the oxidation products, including COO or CO group, indicate carboxylic acids, carboxylates, ketones, and aldehydes. It is reported that FT-IR at 2939, 1400, and 719 form LDPE-TiO2 (1 wt %) samples, when treated with irradiation for 100 h, showed the lower intensity of characteristic alkyl peaks [33]. Similar reports were available by little change from the COO or C = O group, revealing carboxylic acids, carboxylates, ketones, and aldehydes groups [63, 64]. Studies have reported degradation of LDPE using gold nanoparticles showed the formation of phenols, alcohols, ketones, and some smaller compounds [63].

The MS studies of LDPE-ZnO NPs film revealed the liberation of aldehydes, alkenes, cyano compounds, esters, and alkanes with OH, CH_2 C–C, and C-O stretching observed in the chromatogram, which shows the partial degradation of LDPE as shown in (Fig. 13). These peaks indicate that LDPE-ZnO NPs have the potential for complete photodegradation of LDPE into CO_2, with liberations of compounds such as methane, ethene, ethane, propane, propenyl ester of carbonic acid, respectively. Similar reports were observed by [65].

4 Conclusion

As there is a growing urge for eco-friendly protocols to synthesize metal nanoparticles for biomedical uses, low-cost, eco-friendly, simple methods using plant extract have been utilized. In the present study, a simple ZnO NPs synthesis using areca nut extract was demonstrated to be an excellent antibacterial agent. Further, it is revealed that green synthesized ZnO NPs can efficiently inhibit and disrupt the biofilms formed by *E. coli*. The biosynthesized ZnO NPs were found to degrade harmful textile dyes which are present in contaminated water through the photocatalytic activity because of the contribution of superoxides and hydroxyl

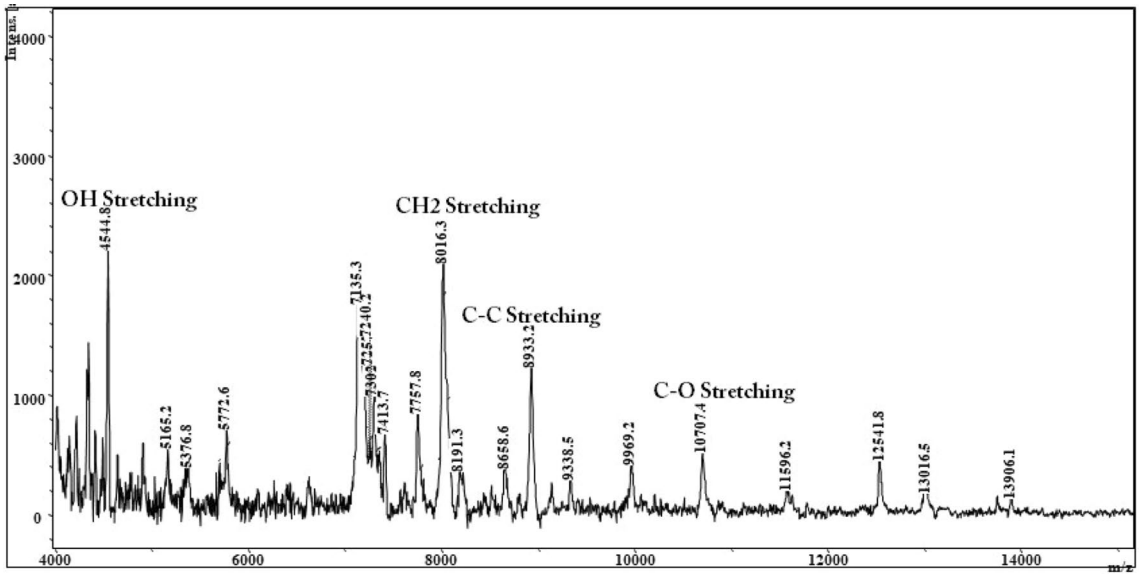

Fig. 13 The MS studies of the LDPE-ZnONPs nanocomposite film revealed the liberation of aldehydes, alkenes, cyanocompounds, esters and alkanes in LDPE

radicals that form during photocatalysis. On the other hand, plastic pollutants like residual LDPE films will be degraded by capping the molecules through the green synthesis of ZnO nanoparticles that could be a viable way for degrading plastics in water using sunlight. Finally, it concludes that the capping of the molecules through the green synthesis of ZnO nanoparticles has been greatly documented for antibacterial, antibiofilm, removal of dyes and plastics can be implicated in the application in the food industry, environmental, hospital, and wastewater treatment.

References

1. T.K. Das, S. Ganguly, P. Bhawal, S. Remanan, S. Mondal, N.C. Das, Mussel inspired green synthesis of silver nanoparticles-decorated halloysite nanotube using dopamine: characterization and evaluation of its catalytic activity. Appl. Nanosci. **8**(1), 173–186 (2018)
2. S. Ganguly, P. Bhawal, R. Ravindren, N.C. Das, Polymer nanocomposites for electromagnetic interference shielding: a review. J. Nanosci. Nanotechnol. **18**(11), 7641–7669 (2018)
3. A.A. Yaqoob, T. Parveen, K. Umar, M.N. Mohamad Ibrahim, Role of nanomaterials in the treatment of wastewater: A review. Water **12**(2), 495 (2020)
4. Y. Orhan, H. Buyukgungor, Enhancement of biodegradability of disposable polyethylene in controlled biological soil. Int. Biodeter. Biodegrad. **45**, 49–55 (2000)
5. Y. Wu, H. Pang, Y. Liu, X. Wang, S. Yu, D. Fu, X. Wang, Environmental remediation of heavy metal ions by novel-nanomaterials: a review. Environ. Pollut. **246**, 608–620 (2019)
6. S.S. Joshi, P.R. Patil, M.S. Nimase, P.P. Bakare, Role of ligands in the formation, phase stabilization, structural and magnetic properties of α-Fe 2 O 3 nanoparticles. J. Nanopart. Res. **8**(5), 635–643 (2006)
7. X.L. Cheng, H. Zhao, L.H. Huo, S. Gao, J.G. Zhao, ZnO nanoparticulate thin film: preparation, characterization and gas-sensing property. Sens. Actuators, B Chem. **102**(2), 248–252 (2004)
8. S.Y. Lee, E.S. Shim, H.S. Kang, S.S. Pang, J.S. Kang, Fabrication of ZnO thin film diode using laser annealing. Thin Solid Films **473**(1), 31–34 (2005)
9. J. Santhoshkumar, S.V. Kumar, S. Rajeshkumar, Synthesis of zinc oxide nanoparticles using plant leaf extract against urinary tract infection pathogen. Resource-Efficient Technol. **3**(4), 459–465 (2017)
10. H. Chandra, D. Patel, P. Kumari, J.S. Jangwan, S. Yadav, Phyto-mediated synthesis of zinc oxide nanoparticles of Berberis aristata: Characterization, antioxidant activity and antibacterial activity with special reference to urinary tract pathogens. Mater. Sci. Eng. C, Mater. Biol. Appl. **102**, 212–220 (2019). https://doi.org/10.1016/j.msec.2019.04.035
11. J.L. Gomez, O. Tigli, Zinc oxide nanostructures: from growth to application. J. Mater. Sci. **48**(2), 612–624 (2013)
12. Q. Zhang, C.S. Dandeneau, X. Zhou, G. Cao, ZnO nanostructures for dye-sensitized solar cells. Adv. Mater. **21**(41), 4087–4108 (2009)
13. S.A. Ansari, M.M. Khan, M.O. Ansari, J. Lee, M.H. Cho, Biogenic synthesis, photocatalytic, and photoelectrochemical performance of Ag–ZnO nanocomposite. J. Phys. Chem. C **117**(51), 27023–27030 (2013)
14. V. Rajendar, C.S. Chakra, B. Rajitha, K.V. Rao, M.C. Sekhar, B.P. Reddy, S.H. Park, Effect of TWEEN 80 on the morphology and antibacterial properties of ZnO nanoparticles. J. Mater. Sci.: Mater. Electron. **28**(4), 3272–3277 (2017)
15. L. Shkodenko, I. Kassirov, E. Koshel, Metal oxide nanoparticles against bacterial biofilms: perspectives and limitations. Microorganisms **8**(10), 1545 (2020)
16. M. Naseer, U. Aslam, B. Khalid, B. Chen, Green route to synthesize zinc oxide nanoparticles using leaf extracts of *Cassia fistula* and *Melia azadarachta* and their antibacterial potential. Sci. Rep. **10**(1), 1–10 (2020)

17. P. Kuppusamy, M.M. Yusoff, G.P. Maniam, N. Govindan, Biosynthesis of metallic nanoparticles using plant derivatives and their new avenues in pharmacological applications–An updated report. Saudi Pharmaceutical Journal **24**(4), 473–484 (2016)
18. S. Ganguly, S. Mondal, P. Das, P. Bhawala T. Das, M. Bose, S. Choudhary, S. Gangopadhyay, A.K. Das, N.C. Das, Natural saponin stabilized nano-catalyst as efficient dye-degradation catalyst. Nano-Struct. Nano-Objects **16**, 86–95 (2018)
19. Y. Chavan, R.S. Singhal, Ultrasound-assisted extraction (UAE) of bioactives from arecanut (*Areca catechu* L.) and optimization study using response surface methodology. Innov. Food Sci. Emerg. Technol. **17**, 106–113 (2013)
20. U.R. Shwetha, M.S. Latha, C.R. Rajith Kumar, M.S. Kiran, V.S. Betageri, Facile synthesis of zinc oxide nanoparticles using novel Areca catechu leaves extract and their in vitro antidiabetic and anticancer studies. J. Inorg. Organometa. Poly. Mater. **30**, 4876–4883 (2020)
21. S.N.A.M. Sukri, K. Shameli, M.M.T. Wong, S.Y. Teow, J. Chew, N.A. Ismail, Cytotoxicity and antibacterial activities of plant-mediated synthesized zinc oxide (ZnO) nanoparticles using *Punica granatum* (pomegranate) fruit peels extract. J. Mol. Struct. **1189**, 57–65 (2019)
22. Y.A. Selim, M.A. Azb, I. Ragab, M.H. Abd El-Azim, Green synthesis of zinc oxide nanoparticles using aqueous extract of *Deverra tortuosa* and their cytotoxic activities. Sci. Rep. **10**(1), 1–9 (2020)
23. N. Sunayana, M. Uzma, R.P. Dhanwini, M. Govindappa, H.S. Prakash, B.V. Raghavendra, Green synthesis of gold nanoparticles from Vitex negundo leaf extract to inhibit lipopolysaccharide-induced inflammation through in vitro and in vivo. J. Cluster Sci. **31**(2), 463–477 (2020)
24. W.R. Diao, Q.P. Hu, S.S. Feng, W.Q. Li, J.G. Xu, Chemical composition and antibacterial activity of the essential oil from green huajiao (*Zanthoxylum schinifolium*) against selected foodborne pathogens. J. Agric. Food Chem. **61**, 6044–6049 (2013). https://doi.org/10.1021/jf4007856
25. H. Bagur, S.M. Raja, S. Prathap, C.P.W. Jayakumar, S.K. Chetan, K.G. Praveen, M. Govindappa, C.P. Chandrappa, Endophyte fungal isolate mediated biogenic synthesis and evaluation of biomedical applications of silver nanoparticles. Mater. Technol. **2020**, 1–12 (2020)
26. A. Nanda, M. Saravanan, Biosynthesis of silver nanoparticles from *Staphylococcus aureus* and its antimicrobial activity against MRSA and MRSE. Nanomed. Nanotechnol. Biol. Med. **5**(4), 452–456 (2009)
27. J.B. Dos Santos Rodrigues, R.J. de Carvalho, N.T. de Souza, K. de Sousa Oliveira, O.L. Franco, D. Schaffner, M. Magnani, Effects of oregano essential oil and carvacrol on biofilms of *Staphylococcus aureus* from food-contact surfaces. Food Control **73**, 1237–1246 (2017)
28. S.Ş Dogan, A. Kocabaş, Green synthesis of ZnO nanoparticles with *Veronica multifida* and their antibiofilm activity. Hum. Exp. Toxicol. **39**(3), 319–327 (2020)
29. A. Pugazhendhi, R. Prabhu, K. Muruganantham, R. Shanmuganathan, S. Natarajan, Anticancer, antimicrobial and photocatalytic activities of green synthesized magnesium oxide nanoparticles (MgONPs) using aqueous extract of *Sargassum wightii*. J. Photochem. Photobiol., B **190**, 86–97 (2019)
30. U. Zhao, X. Li, Y. Chen, L. Shi, Y. Zhu, Solid-phase photocatalytic degradation of polyethylene plastic under UV and solar light irradiation. J. Mol. Catal. A: Chem. **268**(1–2), 101–106 (2007)
31. A.A. Olajire, A.A. Mohammed, Bio-directed synthesis of gold nanoparticles using *Ananas comosus* aqueous leaf extract and their photocatalytic activity for LDPE degradation. Adv. Powder Technol. **32**(2), 600–610 (2021)
32. V.B. Raghavendra, M. Uzma, M. Govindappa, R.A. Vasantha, S. Lokesh, Screening and identification of polyurethane (PU) and low density polyethylene (LDPE) degrading soil fungi isolated from municipal solid waste. Int J Curr Res **8**, 34753–34761 (2016)
33. A. Gupta, P.Y. Lakshmi, R. Manivannan, S.N. Victoria, Visible range photocatalysts for solid phase photocatalytic degradation of polyethylene and polyvinyl chloride. J. Chil. Chem. Soc. **62**(1), 3393–3398 (2017)
34. N. Sauro Bianchi, G. Alexia, K. Ivana, M. Ingo, P. Frederic, Analysis of the structure of condensed tannins in water extracts from bark tissues of Norway spruce (*Picea abies* [Karst.]) and Silver fir (*Abies alba* [Mill.]) using MALDI-TOF mass spectrometry. Ind. Crops Prod. **61**, 430–437 (2014)
35. P. Rajiv, S. Rajeshwari, R. Venckatesh, Bio-Fabrication of zinc oxide nanoparticles using leaf extract of *Parthenium hysterophorus* L. and its size-dependent antifungal activity against plant fungal pathogens. Spectrochim. Acta Part A Mol. Biomol. Spectrosc. **112**, 384–387 (2013)
36. K. Natarajan, S. Selvaraj, V.R. Murty, Microbial production of silver nanoparticle. Digest J. Nanomat. Biostruct. **5**, 135–140 (2010)
37. P. Amuthavalli, J.S. Hwang, H.U. Dahms, L. Wang, J. Anitha, M. Vasanthakumaran, S. Singh, Zinc oxide nanoparticles using plant *Lawsonia inermis* and their mosquitocidal, antimicrobial, anticancer applications showing moderate side effects. Sci. Rep. **11**(1), 1–13 (2021)
38. D. Barrera, N. Pino, D. López, R. Buitrago-Sierra, Reliable preparation of ZnO nanoparticles by different synthesis methods for bactericidal applications. Adv. Nat. Sci.: Nanosci. Nanotechnol. **11**(2), 025015 (2020)
39. K.A. Priyadarshini, K. Murugan, C. Panneerselvam, S. Ponarulselvam, J.S. Hwang, M. Nicoletti, Biolarvicidal and pupicidal potential of silver nanoparticles synthesized using *Euphorbia hirta* against *Anopheles stephensi* Liston (Diptera: Culicidae). Parasitol. Res. **111**(3), 997–1006 (2012)
40. S.S. Shankar, A. Rai, A. Ahmad, M. Sastry, Rapid synthesis of Au, Ag, and bimetallic Au core–Ag shell nanoparticles using Neem (*Azadirachta indica*) leaf broth. J. Colloid Interface Sci. **275**(2), 496–502 (2004)
41. L. Zhang, Y. Jiang, Y. Ding, M. Povey, D. York, Investigation into the antibacterial behaviour of suspensions of ZnO nanoparticles (ZnO nanofluids). J Nanopart Res. **9**, 479–489 (2007)
42. K.M. Rao, A. Kumar, A. Haider, S.S. Han, Polysaccharides based antibacterial polyelectrolyte hydrogels with silver nanoparticles. Mater. Lett. **184**, 189–192 (2016)
43. A. Haider, S. Haider, I.K. Kang, A. Kumar, M.R. Kummara, T. Kamal, S.S. Han, A novel use of cellulose based filter paper containing silver nanoparticles for its potential application as wound dressing agent. Int. J. Biol. Macromol. **108**, 455–461 (2018)
44. Q. Lv, B. Zhang, X. Xing, Y. Zhao, R. Cai, W. Wang, Q. Gu, Biosynthesis of copper nanoparticles using Shewanella loihica PV-4 with antibacterial activity: Novel approach and mechanisms investigation. J. Hazard. Mater. **347**, 141–149 (2018)
45. M.M. Abdel-Kareem, A.A. Zohri, Extracellular mycosynthesis of gold nanoparticles using Trichoderma hamatum: optimization, characterization and antimicrobial activity. Lett. Appl. Microbiol. **67**(5), 465–475 (2018)
46. C. de la Fuente-Núñez, F. Reffuveille, E.F. Haney, S.K. Straus, R.E.W. Hancock, Broad-spectrum anti-biofilm peptide that targets a cellular stress response. PLoS Pathog. **10**, e1004152 (2014). https://doi.org/10.1371/journal.ppat.1004152
47. Y.H. Hsueh, W.J. Ke, C.T. Hsieh, K.S. Lin, D.Y. Tzou, C.L. Chiang, ZnO nanoparticles affect *Bacillus subtilis* cell growth and biofilm formation. PLoS ONE **10**(6), e0128457 (2015)
48. M. Alavi, N. Karimi, Antiplanktonic, antibiofilm, antiswarming motility and antiquorum sensing activities of green synthesized Ag–TiO2, TiO2–Ag, Ag–Cu and Cu–Ag nanocomposites against

multi-drug-resistant bacteria. Artificial Cells, Nanomedicine, and Biotechnology **46**(sup3), S399–S413 (2018)
49. M. Govindappa, S. Tejashree, V. Thanuja, B. Hemashekhar, C. Srinivas, O. Nasif, V.B. Raghavendra, Pomegranate fruit fleshy pericarp mediated silver nanoparticles possessing antimicrobial, antibiofilm formation, antioxidant, biocompatibility and anticancer activity. J. Drug Delivery Sci. Technol. **61**, 102289 (2021)
50. S. Arokiyaraj, S. Vincent, M. Saravanan, Y. Lee, Y.K. Oh, K.H. Kim, Green synthesis of silver nanoparticles using *Rheum palmatum* root extract and their antibacterial activity against *Staphylococcus aureus* and *Pseudomonas aeruginosa*. Artificial Cells, Nanomedicine, and Biotechnology **45**(2), 372–379 (2017)
51. S. Ganguly, P. Das, T.K. Das, S. Ghosh, S. Das, M. Bose, N.C. Das, Acoustic cavitation assisted destratified clay tactoid reinforced in situ elastomer-mimetic semi-IPN hydrogel for catalytic and bactericidal application. Ultrason. Sonochem. **60**, 104797 (2020)
52. K.M.A.E. Fattah, A. Gamal, S. Ibrahim, E.L.M.G. Mohamed, A. Saleh, Investigation of the efficacy of synthesized silver and zinc oxide nanoparticles against multi-drug resistant gram negative bacterial clinical isolates. Arch Clin Microbiol **8**(6), 67 (2017)
53. Rajabairavi, N., Raju, C. S., Karthikeyan, C., Varutharaju, K., Nethaji, S., Hameed, A. S. H., & Shajahan, A. (2017) Biosynthesis of novel zinc oxide nanoparticles (ZnO NPs) using endophytic bacteria *Sphingobacterium thalpophilum* In *Recent Trends in Materials Science and Applications* (pp. 245–254). Springer Cham
54. S. Liu, E. Killen, M. Lim, C. Gunawan, R. Amal, The effect of common bacterial growth media on zinc oxide thin films: identification of reaction products and implications for the toxicology of ZnO. RSC Adv **4**, 4363–4370 (2014)
55. M. Khan, P. Ware, N. Shimpi, Synthesis of ZnO nanoparticles using peels of *Passiflora foetida* and study of its activity as an efficient catalyst for the degradation of hazardous organic dye. SN Applied Sciences **3**(5), 1–17 (2021)
56. T.K. Das, S. Ganguly, P. Bhawal, S. Remanan, S. Ghosh, N.C. Das, A facile green synthesis of silver nanoparticles decorated silica nanocomposites using mussel inspired polydopamine chemistry and assessment its catalytic activity. J. Environ. Chem. Eng. **6**(6), 6989–7001 (2018)
57. T.K. Das, S. Remanan, S. Ghosh, S.K. Ghosh, N.C. Das, Efficient synthesis of catalytic active silver nanoparticles illuminated cerium oxide nanotube: A mussel inspired approach. Environ. Nanotechnol., Monitoring & Management **15**, 100411 (2021)
58. S. Faisal, H. Jan, S.A. Shah, S. Shah, A. Khan, M.T. Akbar, S. Syed, Green synthesis of zinc oxide (ZnO) nanoparticles using aqueous fruit extracts of Myristica fragrans: their characterizations and biological and environmental applications. ACS Omega **6**(14), 9709–9722 (2021)
59. N. Balazs, K. Mogyorosi, D.F. Sranko, A. Pallagi, T. Alapi, A. Oszko, P. Sipos, The effect of particle shape on the activity of nanocrystalline TiO2 photocatalysts in phenol decomposition. Appl. Catal. B **84**(3–4), 356–362 (2008)
60. W. Fa, C. Yang, C. Gong, T. Peng, L. Zan, Enhanced photodegradation efficiency of polyethylene-TiO2nanocomposite film with oxidized polyethylene wax. J. Appl. Polym. Sci. **118**(1), 378–384 (2010)
61. S.S. Ali, I.A. Qazi, M. Arshad, Z. Khan, T.C. Voice, C.T. Mehmood, Photocatalytic degradation of low density polyethylene (LDPE) films using titania nanotubes. Environ. Nanotechnol. Monitoring & Manag. **5**, 44–53 (2016)
62. D. Ponnamma, J.J. Cabibihan, M. Rajan, S.S. Pethaiah, K. Deshmukh, J.P. Gogoi, C. Cheng, Synthesis, optimization and applications of ZnO/polymer nanocomposites. Mater. Sci. Eng., C **98**, 1210–1240 (2019)
63. Y.J. Zhu, N. Olson, T.P. Beebe, Surface chemical characterization of 2.5-μm particulates (PM2. 5) from air pollution in salt lake city using TOF-SIMS, XPS, and FTIR. Environ. Sci. Technol. **35**(15), 3113–3121 (2001)
64. M.M. Chehimi, M.L. Abel, J.F. Watts, R.P. Digby, Surface chemical and thermodynamic properties of γ-glycidoxypropyltrimethoxysilane-treated alumina: an XPS and IGC study. J. Mater. Chem. **11**(2), 533–543 (2001)
65. J. Vijayasree, M.P. Uma, Studying the effect of biosilver nanoparticles on polyethylene degradation. Appl. Nanosci. **9**(3), 491–504 (2018)